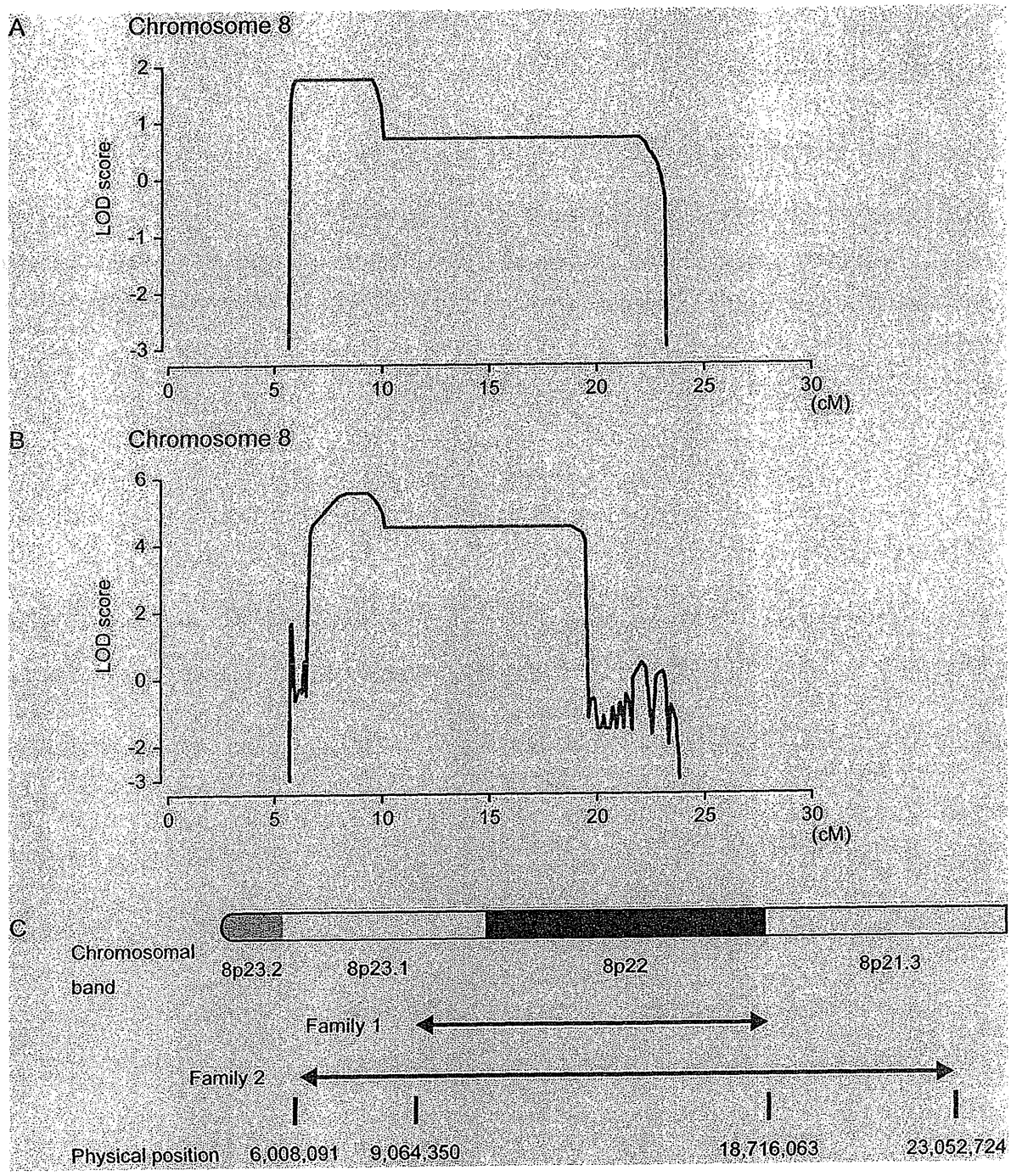

Figure S1. Linkage Analysis and Haplotype Analysis of Family 2

(A) Result of parametric multipoint analysis of Family 2. (B) Cumulative parametric multipoint LOD scores of Families 1 and 2. (C) Candidate regions based on the parametric analysis of Families 1 and 2.

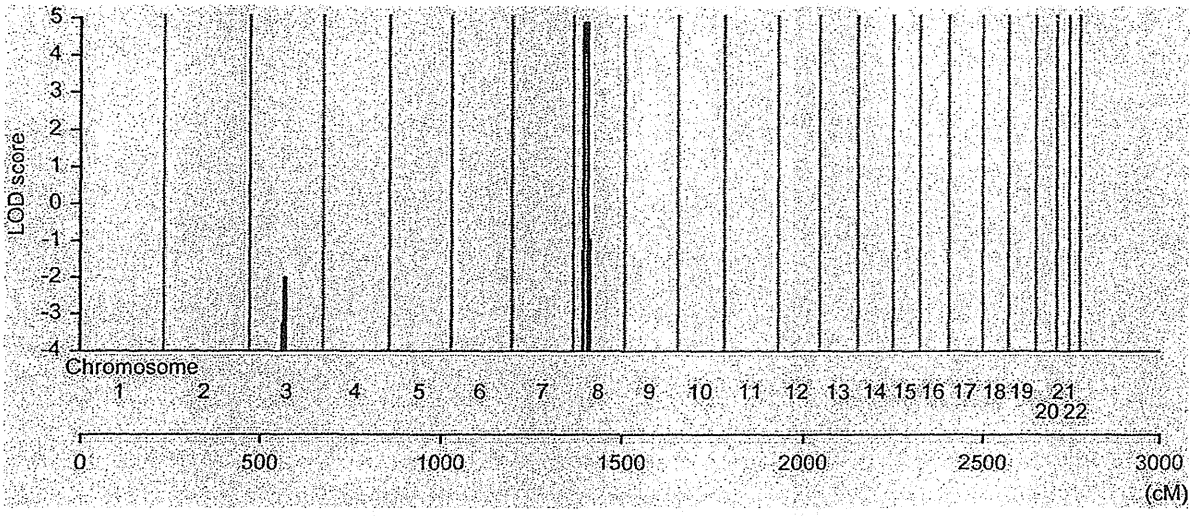

Figure S2. Parametric Linkage Analysis of Families 1 and 2 Using Affected Individuals Only

Cumulative maximum multipoint parametric lod score is shown. Horizontal axis represents the cumulative map position (cM) on the chromosomes 1-22. Family 1 was divided into 2 branches for calculation of LOD score as indicated.

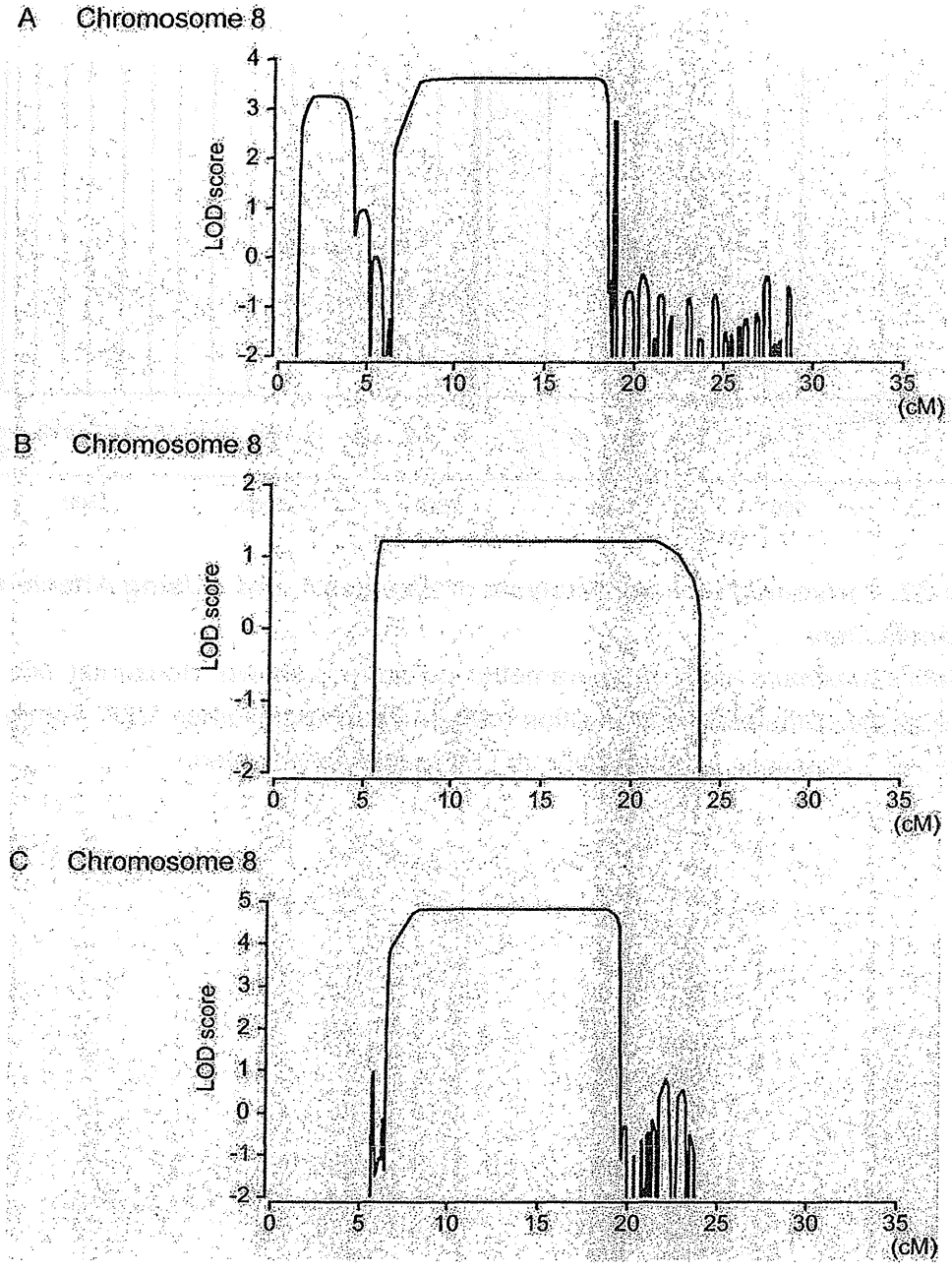

Figure S3. Parametric Linkage Analysis (Affected Individuals Only) at Loci on the Short Arm of Chromosome 8

Only the phenotypes of affected individuals are explicitly indicated in the analysis, while those of other individuals are indicated as "unknown". Maximum multipoint parametric lod scores for Families 1 (A) and 2 (B), and cumulative lod score for Families 1 and 2 (C) are shown. Since the family structure of Family 1 was too large for calculation, the family structure was divided into 2 branches for calculation of LOD score as indicated. Horizontal axis is the map position (cM) on the short arm of chromosome 8.

Table S1. Natural Variant in RP1L1 Sequence in OMD Families

cDNA change	Amino acid change	dbSNP.ID	Number of observed mutations/affected subjects (frequency)	Number of observed mutations/unaffected subjects (frequency)
c.518 G>C	E97Q	ss252841181	0/ 12 (0.00)	1/ 21 (0.05)
c.730 A>G	T167 synonymous	rs79329877	2/ 10 (0.20)	1/ 20 (0.05)
c.894 A>C	H222P	rs4388421	5/ 12 (0.42)	5/ 21 (0.24)
c.1769 G>A	G514S	rs74990397	3/ 12 (0.25)	3/ 21 (0.14)
c.2020 C>T	G597 synonymous	rs6996950	12/ 12 (1.00)	21/ 21 (1.00)
c.2497 C>T	N756 synonymous	rs57819090	4/ 12 (0.33)	3/ 21 (0.14)
c.2604 T>C	L792P	rs35602868	3/ 12 (0.25)	3/ 21 (0.14)
c.2807 C>T	R860W	rs62490856	3/ 12 (0.25)	2/ 21 (0.10)
c.3665 C>T	R1146W	rs4840502	12/ 12 (1.00)	21/ 21 (1.00)
c.4630 G>T	R1467S	rs4840498	12/ 12 (1.00)	21/ 21 (1.00)
c.4677 C>T	A1483V	rs62490855	1/ 12 (0.08)	0/ 21 (0.00)
c.4713 C>G	P1495R	rs4841399	10/ 12 (0.83)	21/ 21 (1.00)
c.5182 G>A	A1659 synonymous	ss252841182	1/ 12 (0.08)	3/ 21 (0.14)
c.5355 C>T	A1709V	rs13267180	3/ 12 (0.25)	3/ 21 (0.14)
c.5895 A>T	D1889V	rs28446662	9/ 12 (0.75)	18/ 19 (0.95)
c.6647 G>A	E2140K	rs72494282	5/ 12 (0.42)	5/ 21 (0.24)
c.6740 G>A	E2171K	rs4354268	2/ 12 (0.17)	1/ 21 (0.05)
c.6952 A>G	S2241 synonymous	rs56382513	11/ 12 (0.92)	20/ 21 (0.95)
c.7082 G>A	G2285R	rs55642448	11/ 12 (0.92)	21/ 21 (1.00)

Nucleotides and amino acid are numbered as in GenBank accesssion number NM_178857 and NP_849188.4, respectively. Sequencing of the CDS excluding repeat site (approximately 3960 to 4320 and 5980 to 6480; NM_178857) of RP1L1 in OMD family members.

OPEN ACCESS Freely available online

PLoS one

Modeling Retinal Degeneration Using Patient-Specific Induced Pluripotent Stem Cells

Zi-Bing Jin[1,2☯], Satoshi Okamoto[1☯], Fumitaka Osakada[3], Kohei Homma[1], Juthaporn Assawachananont[1], Yasuhiko Hirami[1], Takeshi Iwata[4], Masayo Takahashi[1,5]*

1 Laboratory for Retinal Regeneration, RIKEN Center for Developmental Biology, Kobe, Japan, **2** School of Optometry and Ophthalmology, Eye Hospital, Wenzhou Medical College, Wenzhou, China, **3** Systems Neurobiology Laboratory, The Salk Institute for Biological Studies, La Jolla, California, United States of America, **4** National Institute of Sensory Organs, National Hospital Organization Tokyo Medical Center, Tokyo, Japan, **5** Center for iPS Research and Application, Kyoto University, Kyoto, Japan

Abstract

Retinitis pigmentosa (RP) is the most common inherited human eye disease resulting in night blindness and visual defects. It is well known that the disease is caused by rod photoreceptor degeneration; however, it remains incurable, due to the unavailability of disease-specific human photoreceptor cells for use in mechanistic studies and drug screening. We obtained fibroblast cells from five RP patients with distinct mutations in the *RP1*, *RP9*, *PRPH2* or *RHO* gene, and generated patient-specific induced pluripotent stem (iPS) cells by ectopic expression of four key reprogramming factors. We differentiated the iPS cells into rod photoreceptor cells, which had been lost in the patients, and found that they exhibited suitable immunocytochemical features and electrophysiological properties. Interestingly, the number of the patient-derived rod cells with distinct mutations decreased *in vitro*; cells derived from patients with a specific mutation expressed markers for oxidation or endoplasmic reticulum stress and exhibited different responses to vitamin E than had been observed in clinical trials. Overall, patient derived rod cells recapitulated the disease phenotype and expressed markers of cellular stresses. Our results demonstrate that the use of patient-derived iPS cells will help to elucidate the pathogenic mechanisms caused by genetic mutations in RP.

Citation: Jin Z-B, Okamoto S, Osakada F, Homma K, Assawachananont J, et al. (2011) Modeling Retinal Degeneration Using Patient-Specific Induced Pluripotent Stem Cells. PLoS ONE 6(2): e17084. doi:10.1371/journal.pone.0017084

Editor: Mark Mattson, National Institute on Aging Intramural Research Program, United States of America

Received October 28, 2010; **Accepted** January 15, 2011; **Published** February 10, 2011

Funding: This study was supported by the grant from the Ministry of Health, Labour and Welfare, Japan (#H21-Nanchi-Ippan-216). The funders had no role in study design, data collection and analysis, decision to publish, or preparation of the manuscript.

Competing Interests: The authors have declared that no competing interests exist.

* E-mail: mretina@cdb.riken.jp

☯ These authors contributed equally to this work.

Introduction

Retinitis pigmentosa (RP) leads inevitably to visual impairment due to irreversible retinal degeneration, specifically of primary rod photoreceptors. The condition causes night blindness and visual field defects. The disease onset spans a wide range of ages, but RP most often occurs in late life. There is no treatment that allows patients to avoid deterioration of visual function. RP encompasses a number of genetic subtypes, with more than 45 causative genes and a large number of mutations identified thus far. The genetic heterogeneity of RP suggests a diversity of disease mechanisms, which remain largely unclear. Furthermore, for many of the RP subtypes, no appropriate animal models are available. Although large clinical trials have been conducted with α-tocopherol and β-carotene, these studies found no statistically significant change of visual function in RP patients [1,2]. The underlying mutations causing disease in the patients tested in the clinical trials were not revealed, and the variability of individual responses to these drugs is unknown. One of the reasons why these clinical trials failed to examine the effectiveness of drugs is that the effect of a drug may be different between patients with different underlying mutations.

Induced pluripotent stem (iPS) cells reprogrammed from somatic cells [3,4] have enabled us to easily generate patient-derived terminally differentiated cells *in vitro* [5–7]. We have successfully induced differentiation of photoreceptor cells from both human embryonic stem (ES) cells [8] and iPS cells [9,10]. Modeling pathogenesis and treatment *in vitro* using patient iPS cell-derived photoreceptors will elucidate disease mechanisms; circumvent problems related to differences among species that arise when using animal models; decrease patient risk; and reduce the cost of early-stage clinical trials. Here, we generated iPS cells from RP patients with different mutations and demonstrated the potential of patient-derived photoreceptors for disease modeling.

Materials and Methods

RP patients and genetic mutations

The protocol of this study adhered to the tenets of the Declaration of Helsinki. The study was approved by the ethical committees of the Institute of Biomedical Research and Innovation Hospital and the RIKEN Center for Developmental Biology, Japan. Written informed consent from all patients was obtained. We selected five RP patients from four families whose disease-causing mutations have been identified (**Fig. 1A–D and Fig. S1**) Of the five RP patients in this study, three late-onset patients carried the following mutations: 721Lfs722X in *RP1*, W316G in *PRPH2*, and G188R in *RHO*. Two relatively early-onset patients from the same family carried a H137L mutation in *RP9*, which we

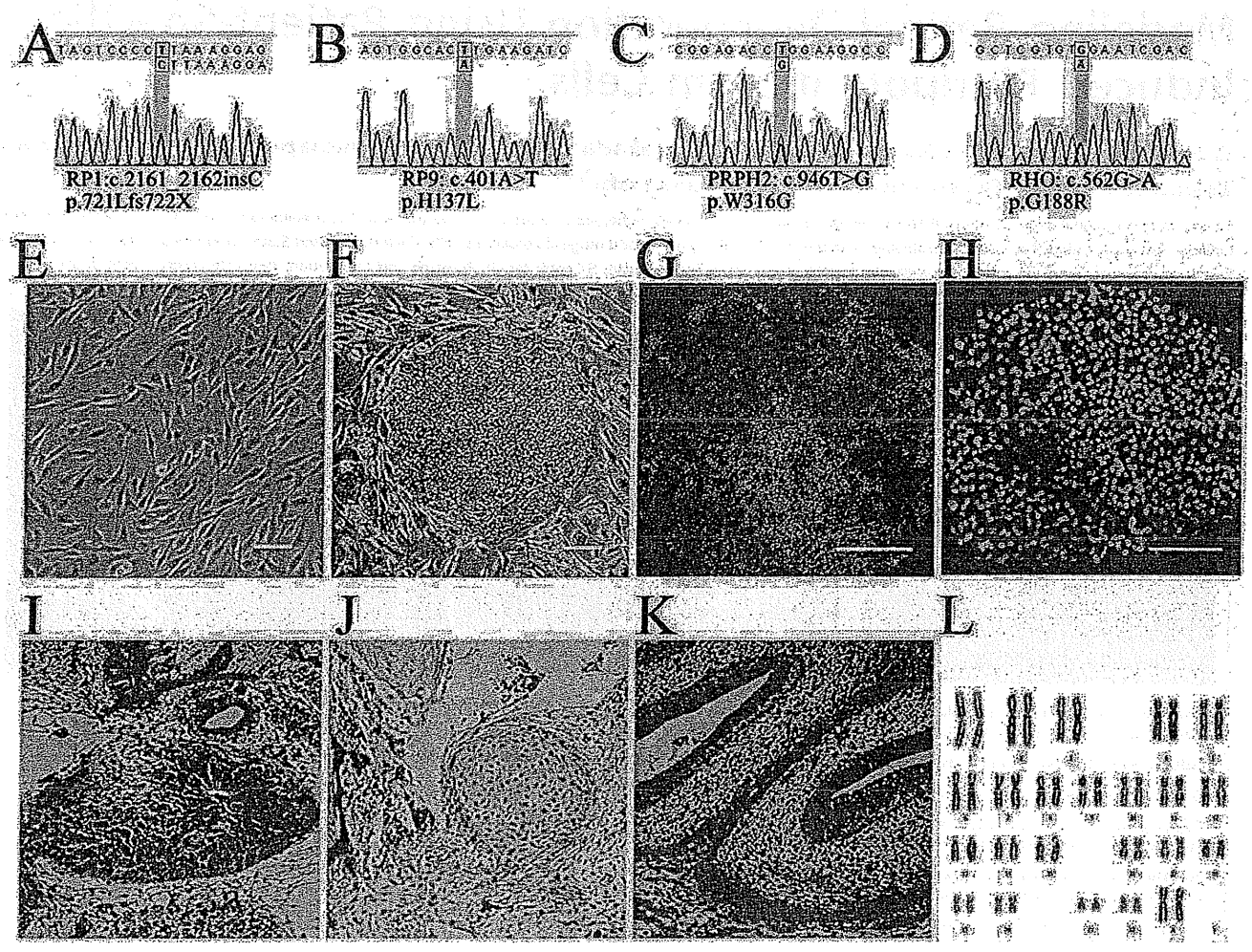

Figure 1. iPS cells derived from RP patients. Mutations identified in patients K21 (RP1) (**A**), K11 and K10 (RP9) (**B**), P101 (PRPH2) (**C**), and P59 (RHO) (**D**). Patient-derived fibroblast cells (**E**) were reprogrammed into iPS cells (**F**). The iPS cells expressed SSEA-4 (**G**) and Nanog (**H**). A teratoma formation test confirmed iPS cells' ability to generate all three germ layers: endoderm (**I**), mesoderm (**J**) and ectoderm (**K**). Karyotype analysis (**I**). Scale bars, 50 μm.
doi:10.1371/journal.pone.0017084.g001

confirmed by both genomic and cDNA sequencing (**Fig. S2**). All patients showed typical manifestations of RP (**Tab. S1**). Peripheral blood obtained from patients was used for DNA isolation. A comprehensive screening of disease-causing genes was carried out as described previously [11]. For the RP9 mutation, total RNA was isolated from fresh blood samples and iPS cells, and synthesized cDNA was subjected to PCR and direct sequencing to confirm whether the mutation was located in the *RP9* gene or the pseudo-RP9 gene (paralogous variant). Both fibroblast and iPS cells were analyzed to re-confirm the identified mutation.

iPS cells generation

To generate iPS cells, retroviral transduction of Oct3/4, Sox2, Klf4, and c-Myc into patient-derived fibroblast cells was carried out as described previously [3]. Established iPS cell lines were maintained on a feeder layer of mitomycin C-treated SNL cells (a murine-derived fibroblast STO cell line expressing the neomycin-resistance gene cassette and LIF) in a humidified atmosphere of 5% CO_2 and 95% air at 37°C. Cells were maintained in DMEM-F12 supplemented with 0.1 mM non-essential amino acids, 0.1 mM 2-mercaptoethanol, 2 mM L-glutamine, 20% KnockOut Serum Replacement (KSR), and 4 ng/ml basic fibroblast growth factor (Upstate Biotechnology).

Transgene quantification

To examine the copy number of transgenes integrated into the host genome, DNA was isolated and quantitative detection of viral transgenes was performed using real-time PCR. The endogenous gene was used as a control. Before quantitative PCR, a standard curve for each primer and/or probe set was determined using a set of plasmid DNA dilutions. Taqman qPCR to detect integrated OCT3/4, KLF4, and MYC was performed using 20 μl reactions consisting of 10 μl TaqMan Master Mix with uracil N-glycosylase, 4.9 μM primers, 250 nM probe, and 1 μl of the DNA sample. Quantification of viral SOX2 was assayed using SYBR Green.

Teratoma formation

Animal protocols were approved by the RIKEN Center for Developmental Biology ethical committee (No. AH18-05). A total of 10^7 trypsinized iPS cells were injected subcapsularly into the testis of SCID mice (two mice per iPS cell line). Four weeks later, the testis was fixed and sectioned for H&E staining.

Immunocytochemistry

Cells were fixed with 4% paraformaldehyde for 15 min at 4°C and then permeabilized with 0.3% Triton X-100 for 45 min. After 1 h blocking with 5% goat serum, cells were incubated with primary antibodies overnight at 4°C and subsequently with secondary antibodies for 1 h at room temperature. The primary and second antibodies used are listed in **Tab. S2**.

Karyotype analysis

Karyotype analysis of the iPS cell chromosomes was carried out using a standard G-band technique (300–400 band level).

Photoreceptor differentiation and drug testing

In vitro differentiation of rod photoreceptor cells was performed as previously reported [8], but with a minor modification. To find a KSR optimal for retinal differentiation, lot testing was conducted before differentiation. iPS colonies were dissociated into clumps with 0.25% trypsin and 0.1 mg/ml collagenase IV in PBS containing 1 mM $CaCl_2$ and 20% KSR. Feeder cells were removed by incubation of the iPS cell suspension on a gelatin-coated dish for 1 h. iPS clumps were moved to a non-adhesive MPC-treated dish (NUNC) in maintenance medium for 3 days, in 20% KSR-containing differentiation medium (DMEM-12 supplemented with 0.1 mM non-essential amino acids, 0.1 mM 2-mercaptoethanol, 2 mM L-glutamine) for 3 days, then in 15% KSR-containing differentiation medium for 9 days, and finally in 10% KSR-containing medium for 6 days. Cells were treated with Lefty-A and Dkk-1 during floating culture. At day 21, the cells were plated en bloc on poly-D-lysine/laminin/fibronectin–coated 8-well culture slides (BD Biocoat) at a density of 15–20 aggregates/cm^2. The cells were cultured in 10% KSR-containing differentiation medium until day 60. Cells were further treated with 100 nM retinoic acid (Sigma) and 100 μM taurine (Sigma) in photoreceptor differentiation medium (GMEM, 5% KSR, 0.1 mM non-essential amino acids, 0.1 mM 2-mercaptoethanol, 1 mM pyruvate, N2 supplement, and 50 units/ml penicillin, 20 μg/ml streptomycin). Differentiated cells from both normal and patient iPS cells were treated with 100 μM α-tocopherol, 200 μM ascorbic acid and 1.6 μM β-carotene starting at differentiation day 120. One week later, cells were fixed for immunostaining.

Electrophysiological recording

Recombinant lentiviral vectors expressing GFP under the control of the Nrl or RHO promoters were generated in HEK293t cells (RIKEN Cell Bank), and differentiated cells were infected with virus on day 90. Cells expressing GFP were targeted for patch clamp recordings. Voltage-clamp recordings were performed with 12–15 MΩ glass electrodes. Signals were amplified using Multiclamp 700B amplifiers (Molecular Devices). The internal solution was 135 mM K-gluconate, 10 mM HEPES, 3 mM KCl, 0.2 mM EGTA, 2.5 mM $MgCl_2$, 5 mM adenosine 5′-triphosphate, 0.3 mM guanosine-5′-triphosphate, 0 06 mM Alexa Fluor 594 (Molecular probes), adjusted to pH 7.6 with KOH. The retinal cells were perfused with oxygen-bubbled external medium: 23 mM $NaHCO_3$, 0 5 mM KH_2PO_4, 120 mM NaCl, 3.1 mM KCl, 6 mM Glucose, 1 mM $MgSO_4$, 2 mM $CaCl_2$, and 0 004% Phenol red. The medium was heated to 37°C with a temperature controller (Warner Instruments)

Cell count and statistical analysis

Differentiated cells visualized with specific antibodies were counted blindly by an independent observer. Data are expressed as means ± s.e.m. The statistical significance of differences was determined by one-way ANOVA followed by Tukey's test or Dunnett's test, or by two-way ANOVA followed by Bonferroni test using the GraphPad Prizm software. Probability values less than 0.05 were considered significant.

Results

Generation of iPS cell lines from patients with RP

Mutations identified in the five patients were confirmed by bi-directional sequencing (**Fig. S1**). Through genotyping of four patients and two normal relatives in the RP9 family, we found the H137L mutation in the *RP9* gene co-segregated with the disease, strongly indicating that the mutation is indeed the genetic cause of the disease. We cultured fibroblasts from skin samples of these patients on gelatin-coated dishes (**Fig. 1E**) and infected them with retroviral vectors encoding *OCT3/4* (also known as *POU5F1*), *SOX2*, *KLF4*, and *c-MYC*, using a previously established method [3]. Each mutation was re-confirmed in both fibroblasts and iPS cells. Established iPS colonies showed human embryonic stem cell-like morphology (**Fig. 1F and Fig. S3A**) and expressed pluripotency markers (**Fig. 1C–D**). We selected iPS cell lines for each patient using multiple criteria. First, we excluded iPS cell lines in which spontaneous differentiation occurred repeatedly during maintenance (**Fig. S3B**). We chose iPS colonies that maintained morphologies similar to those of human ES cells through more than 10 passages. Second, we quantified the transgene copy number and selected iPS cell lines with the fewest integrations, as the risk of gene disruption through random insertion increases with the number of transgenes (**Fig. S4A–E**). Third, in order to select iPS cell lines with full pluripotency, we verified the ability to form teratomas. Teratomas formed by injecting iPS colonies into the testis *in vivo* showed contributions to all three embryonic germ layers: ectoderm, mesoderm, and endoderm (**Fig. 1E–G**). Finally, karyotype analysis was carried out to examine the chromosome integrity. The patient-iPS cells showed normal karyotypes after extended passage, indicating chromosomal stability (**Fig. 1H**). These results provide *in vitro* and *in vivo* functional proof of pluripotency for RP patient-derived iPS cells.

Generation of patient-specific retinal photoreceptor

We previously demonstrated *in vitro* differentiation of retinal photoreceptor cells from wild-type human ES [8] and iPS cells [9,10] using a stepwise differentiation method known as serum-free culture of embryoid body-like aggregates [12]. We first evaluated the differentiation efficiency of three selected iPS cell lines of the five patients (**Fig. 2A**). Retinal progenitor, photoreceptor precursor, retinal pigment epithelium (RPE) and rod photoreceptor cells were sequentially induced (**Fig. 2B–K**), consistent with our previous studies [8–10,12]. All patient-derived iPS cell lines differentiated into RPE cells that form ZO-1+ tight junctions on differentiation day 60, with timing, morphology, and efficiency similar to that of wild-type iPS cells (**Fig. 2D–E; Fig. S5**). Immature photoreceptors expressing Crx and Recoverin (day ~60) were observed as clusters in the colonies (**Fig. S6A–B**). The patient-iPS cells also differentiated into blue Opsin+ or red/green Opsin+ cone photoreceptor cells (**Fig. 2H** and data not shown). Immunostaining of Rhodopsin (a marker of mature rod photoreceptors) revealed no Rhodopsin+ cells at differentiation day 100 (data not shown). Rhodopsin+ cells appeared at differentiation day 120 with a stable efficiency of the three independent iPS cell lines from each patient (**Fig. 2K,N and Fig. S6C**). Additionally, 15.1±0.60% and 13.3±1.65% cells were positive for Recoverin (a conventional marker for both rod, cone photoreceptors and cone bipolar cells) in K21- and K11-iPS cells, respectively

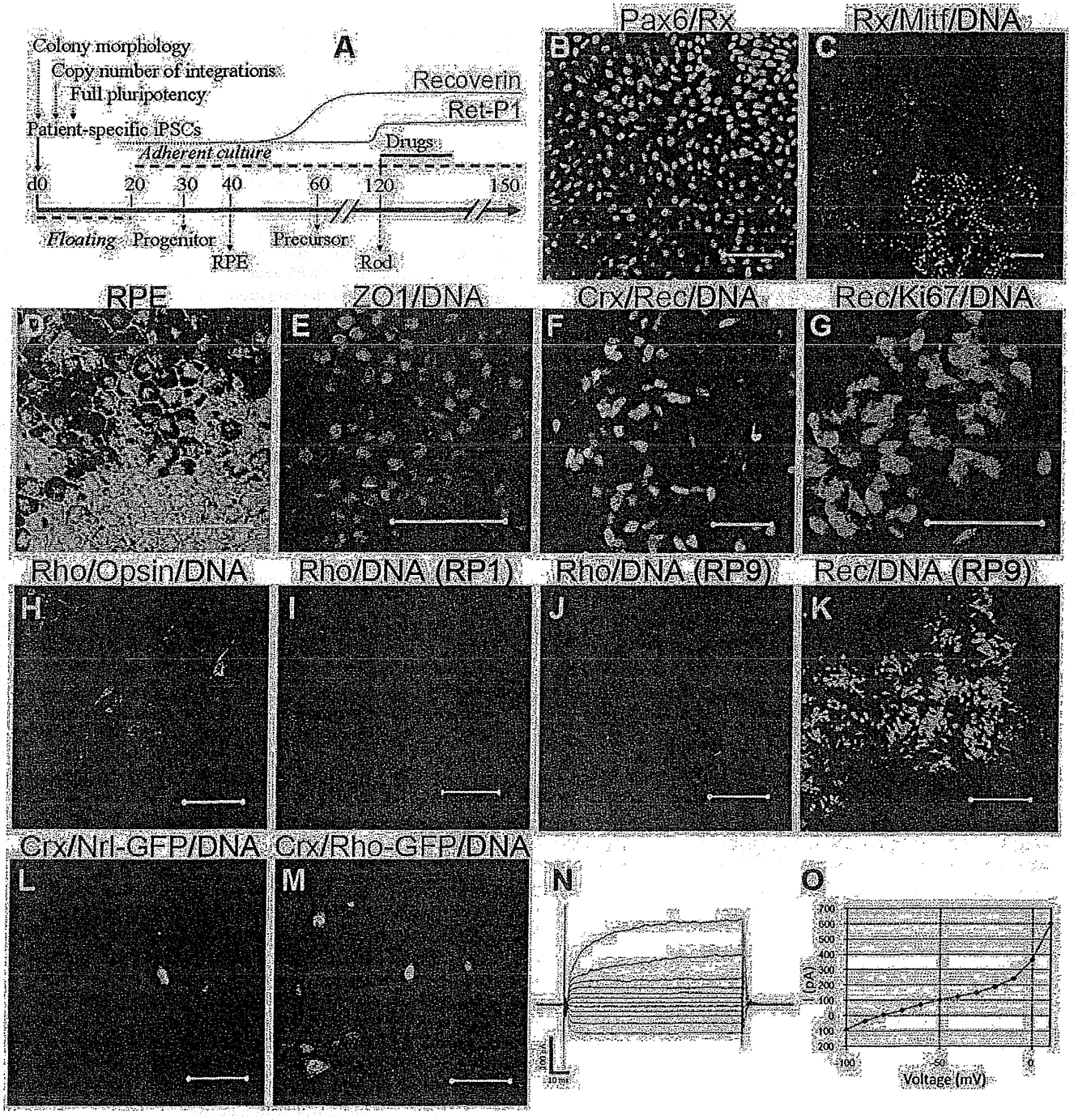

Figure 2. Induction of patient-specific retinal photoreceptor cells. Retinal cells were induced sequentially by *in vitro* differentiation. (**A**) Experimental schema. (**B**) Neural retina progenitor cells (Pax6+Rx+) and RPE progenitor cells (Mitf+) were separated in the culture dish (**C**). Patient-specific RPE cells exhibited hexagonal morphology and pigmentation (**D**) and expressed the tight junction marker ZO-1 (**E**). Photoreceptor cells were positive for immature photoreceptor markers Crx and Recoverin on day 60 (**F**). Recoverin+ cells did not co-express Ki67, a proliferating cell marker (**G**). Differentiation of rod photoreceptors (Rhodopsin+) and cone photoreceptors (Opsin+) from patient iPS cells (**H**). Rhodopsin + rod photoreceptors induced from K21-iPS at day 120 (**I**). K11-derived rod photoreceptors were observed at day 120 (**J**). No Rhodopsin+ cells were detected, but Recoverin+ cells were present at day 150(**K**). Induced rod photoreceptor cells (Crx+) labeled with lentiviral vectors encoding GFP driven by a rod photoreceptor-specific promoter Nrl (**L**: Nrl-GFP) or Rhodopsin (**M**: Rho-GFP). Arrows indicate cells co-expressing Crx and GFP. (**N**) Whole-cell recording of rod photoreceptor cell differentiated human iPS cells. Recorded cells expressed GFP under the control of the Rhodopsin promoter. (**O**) Relationship between voltage and membrane current (i) produced a non-linear curve, suggesting that voltage-dependent channels exist in iPS cell-derived rod photoreceptors Rec, Recoverin; Rho, Rhodopsin. Scale bars, 50 μm.
doi:10.1371/journal.pone.0017084.g002

(data from three selected lines), consistent with stable differentiation. Furthermore, we confirmed rod induction by labeling with lentiviral vectors driving GFP from the Rhodopsin and Nrl promoters, either of which is specifically expressed in rod photoreceptors (**Fig. 2L–M**). Whole-cell patch-clamp recording demonstrated that the rod photoreceptor cell membrane contains voltage-dependent channels, suggesting that differentiated patient-derived rod cells are electrophysiologically functional (**Fig. 2N–O**). Meanwhile, the excluded iPS cell lines (ones that showed spontaneous differentiation during maintenance, or had a high copy number of transgenes), demonstrated a significant diversity of differentiation (**Fig. S7**). Together, these data show that patient-derived iPS cells can differentiate into cells that exhibit many of the immunochemical and electrophysiological features of mature rod photoreceptor cells.

Patient-specific rod cells undergo degeneration *in vitro*

As compared with normal iPS cells, there is no significant difference in rod cell differentiation efficiency at day 120 in K21(RP1)-, P101(PRPH2)-, and P59(RHO)-iPS cell lines (**Fig. 3**). iPS cells from both K11(RP9) and K10(RP9) carried a RP9 mutation; however, rod cell number was significantly lower than in normal iPS cells (**Fig. 3**). We asked whether early death of precursor cells leads to a smaller number of mature rod photoreceptor cells. To determine whether genetic mutations induce degeneration in photoreceptors cells *in vitro*, we extended the culture period and evaluated the number of rod photoreceptors at day 150. In differentiated iPS cells from patient K21(RP1) at day 150, the number of Rhodposin+ cells was significantly decreased (**Fig. 3**). For the K11-iPS cells, no Rhodposin+ cells were found at day 150 (**Fig. 3**). Importantly, some K11-cells at day 150 were positive for Recoverin (10.3±1.99%) and Crx, markers for the rod, cone photoreceptors, and/or bipolar cells (**Fig. 2K** and data not shown), strongly suggesting that cone photoreceptor and/or bipolar cells survived, whereas the rod photoreceptors underwent degeneration *in vitro*. In addition, we detected cells positive for Islet1 (a marker for retinal amacrine, bipolar and ganglion cells), again consistent with the survival of other types of retinal cells (**Fig. S6F**). From these results, we concluded that mature rod photoreceptors differentiated from patient iPS cells selectively degenerate in an RP-specific manner *in vitro*.

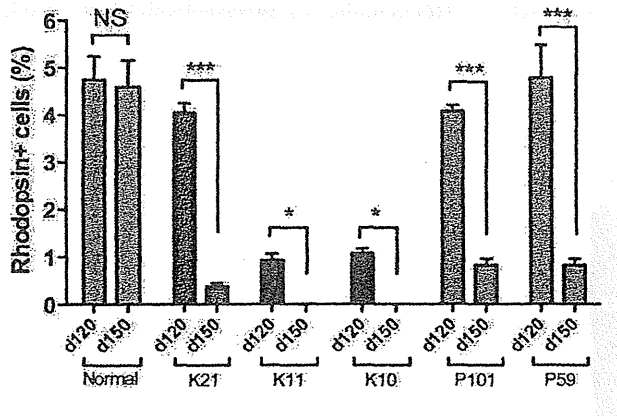

Figure 3. RP patient-derived rod photoreceptors undergo degeneration *in vitro*. iPS cells were differentiated into Rhodopsin+ rod photoreceptors in serum-free culture of embryoid body-like aggregates (SFEB culture). The percentages of Rhodopsin+ rod photoreceptors were evaluated at both day 120 and day 150, respectively. Data were from three independent iPS cell lines derived from the patients. ANOVA followed by Dunnett's test. * $p<0.05$; *** $p<0.001$. Values in the graphs are means and s.e.m.
doi:10.1371/journal.pone.0017084.g003

Cellular stresses involved in patient-derived rod cells

We next asked how the patient-derived rod photoreceptors degenerate. We evaluated apoptosis and cellular stresses in each cell line at both day 100 and day 120, respectively. Interestingly, in the RP9-iPS (K10 and K11) cells, a subset of Recoverin+ cells co-expressed cytoplasmic 8-hydroxy-2'-deoxyguanosine (8-OHdG), a major oxidative stress marker, indicating the presence of DNA oxidation in RP9 patient-derived photoreceptors by differentiation day 100 (**Fig. 4A** and **Fig. S8**). More caspase-3+ cells were presented in the Crx+ photoreceptor cluster of RP9-iPS than in those from other lines (**Fig. 4C–D**). After maturation of the rod photoreceptors from RP9-iPS cells, Rhodopsin+ cells co-expressed Acrolein, a marker of lipid oxidation (**Fig. 4E**), while no Rhodopsin+/Acrolein+ cells were observed in iPS cells derived from other patients carrying different mutations or in normal iPS cells (**Fig. 4F**). This pattern was similar to the cases of 8-OHdG and activated caspase-3. Thus, we conclude that oxidation is involved in the RP9-rod photoreceptor degeneration.

In differentiated RHO-iPS (P59) cells, we found that Rhodopsin proteins were localized in the cytoplasm (**Fig. 4G**), as determined by immunostaining with anti-Rhodopsin antibody (Ret-P1). This pattern is unlike the normal localization of Rhodopsin at the cell membrane in photoreceptors derived from normal iPS or other patient-derived iPS cells (**Fig. 4H** and data not shown). This result suggests accumulation of unfolded Rhodopsin, as reported previously in rhodopsin mutant mice cells [13] We next examined the possible involvement of endoplasmic reticulum (ER) stress in RHO-iPS cell line degeneration. The Rhodopsin+ or Recoverin+ cells co-expressed immunoglobulin heavy-chain binding protein (BiP) or C/EBP homologous protein (CHOP), two conventional markers of endoplasmic reticulum (ER) stress, from day 120 (**Fig. 4I,K and Fig. S9**), while cells derived from control iPS or other mutant iPS cells were negative for BiP and CHOP (**Fig. 4J,L**). Taken together, these results demonstrate that ER stress is involved in rod photoreceptors carrying a RHO mutation.

Drug evaluation in patient-specific rod cells

The antioxidant vitamins α-tocopherol, ascorbic acid, and β-carotene have been tested in clinical trials as dietary therapies for RP [2] and in another major retinal degenerative disease, age-related macular degeneration [14]. Thus far, mostly due to the lack of appropriate validation models, there has been no evidence supporting the beneficial effects of these compounds on rod photoreceptors. We therefore assessed the effects of these agents on rod photoreceptors derived from patient iPS cells. In mouse retinal culture, short-term treatment with α-tocopherol, ascorbic acid and β-carotene at 100 μM, 200 μM and 1.6 μM, respectively, exerted no significant toxic effects on rod photoreceptor cells (**Fig. S10**). Since the differentiated rod photoreceptors underwent degeneration after day 120, we treated the cells for 7 days with these agents starting at day 120 (**Fig. 2A**). α-Tocopherol treatment significantly increased the number of Rhodopsin+ cells in iPS cells derived from K11- and K10-iPS with the RP9 mutation, while it had no significant effects on iPS cells with the either the RP1, PRPH2 or RHO mutation (**Fig. 5**). In contrast, neither ascorbic acid nor β-carotene treatment had any effect on iPS cells of any genotype (**Fig. S11**). We cannot currently explain the discrepancy between the effects of these antioxidants. It has been reported that under certain circumstances, anti-oxidants can act as "pro-oxidants" [15]. Taken together, our results indicate that treatment with α-tocopherol is beneficial to RP9-rod photoreceptor survival, and causes different effects on Rhodposin+ cells derived from different patients.

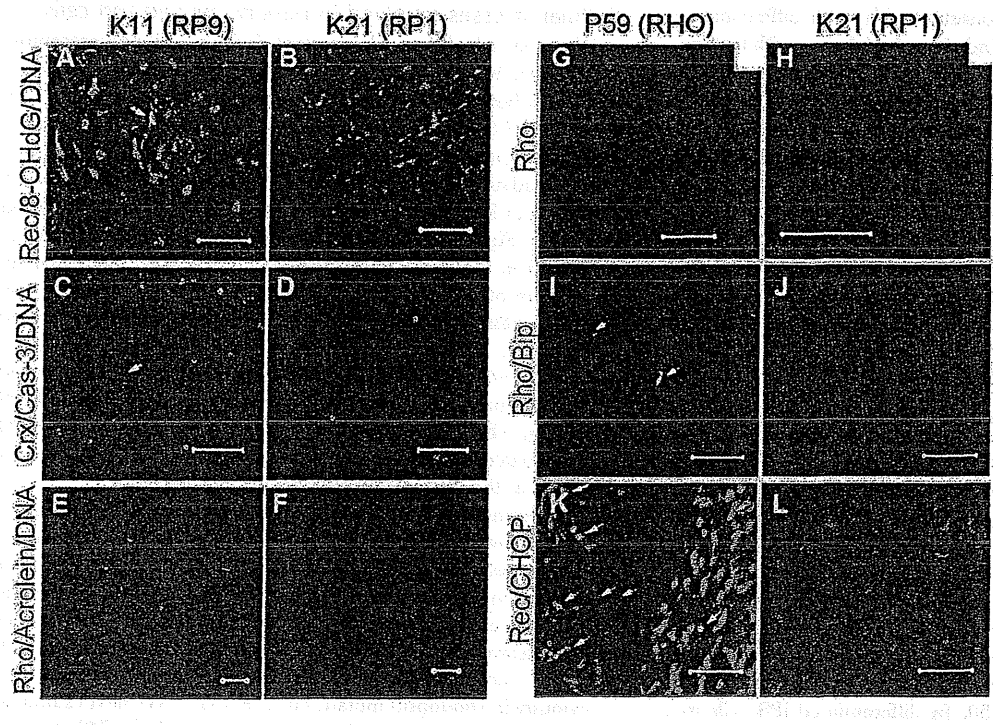

Figure 4. Cellular stress in patient-derived rod photoreceptor cells. Oxidative stress and apoptosis in differentiated rod photoreceptor cells derived from RP9-iPS (**A,C,E**) and RP1-iPS (**B,D,F**). (**A**) 8-OHdG, a marker for DNA oxidation, was found in K11- or K10-iPS–derived differentiated cells (day 100), but not in K21-iPS (**B**). Arrow indicates a cell double-positive for 8-OHdG and Recoverin. (**C**) The number of activated Caspase-3+ cells was greater in K11-iPS differentiation than in K21-iPS (**D**). From day 120, rod photoreceptor cells (Rhodopsin+) derived from RP9-iPS co-expressed the oxidative stress marker Acrolein (**E**); whereas RP1-iPS derivatives did not (**F**). (**G–L**) Abnormal cellular localization of Rhodopsin proteins and endoplasmic reticulum stress in RHO-iPS–derived rod photoreceptors. High magnification revealed cytoplasmic localization of Rhodopsin in rod photoreceptor cells carrying a RHO mutation (**G**) and a normal localization in the cell membrane in K21 cells (**H**). Rod cells derived from RHO-iPS co-expressed the ER stress markers BiP (**I**) and CHOP (**K**). K21-iPS–derived rod cells did not express BiP (**J**) or CHOP (**L**). Arrows indicate double-positive cells. Rec, Recoverin; Rho, Rhodopsin. All scale bars are 50 μm except for G and H (20 μm).
doi:10.1371/journal.pone.0017084.g004

Discussion

By using patient-derived iPS cells and *in vitro* differentiation technology, we have shown that RP9-retinitis pigmentosa is involved, at least in part, in oxidative stress pathways; this has not been reported previously in any animals or cell models. Furthermore, we have demonstrated that the antioxidant α-tocopherol exerts a beneficial effect on RP9-rod cells. Additionally, we have clearly shown that rod photoreceptors derived from patients with a RHO mutation are associated with ER stress; this is

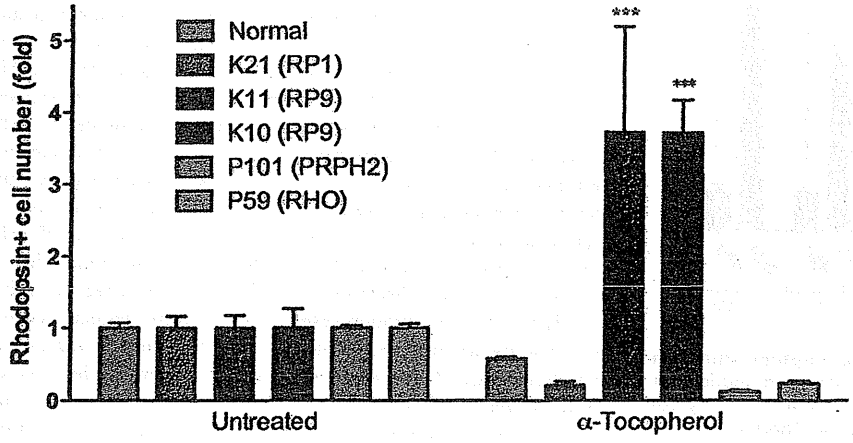

Figure 5. Disease modeling of patient-derived rod photoreceptor cells. α-Tocopherol treatment of patient-specific rod photoreceptors yielded a significant beneficial effect in RP9 mutant cells. Two-way ANOVA Bonferroni post-test showed no significance in other group (n = 3–8). Data represent 1–2 selected iPS cell lines of each patient. ***$p<0.001$. Values in the graphs are means and s.e.m.
doi:10.1371/journal.pone.0017084.g005

the first report of ER stress in a cell culture model for human rod cells. These cell models will be very useful for disease mechanism dissection and drug discovery. By screening several drugs that had already been tested in RP patients, we have revealed that rod photoreceptor cells derived from RP patients with different genetic subtypes exhibit significant differences in drug responses. Among the different types of antioxidants, α-tocopherol has either beneficial or non-beneficial effects on diseased photoreceptors, depending on the genetic mutation. This is the first report of the utilization of iPS cells related to personalized medicine, which will be helpful for routin clinical practice. Our results also provided evidence that genetic diagnosis is essential for optimizing personalized treatment for patients with retinal degenerative diseases [11]. An important future study made possible by this work is the screening of a compound library for drugs that could be used to treat RP. Patient-derived iPS cells revealed differences in pathogenesis and the efficacy of antioxidants among patients with different disease-causing mutations. Although the microenvironment affects the pathogenesis of diseases, and *in vitro* evaluation is not perfect, this study suggests that iPS cells could be used to select between multiple available treatments, allowing physicians to advise each patient individually. The weakness of our method for disease modeling is that differentiation requires a long period of time. Shortening the induction period and identifying appropriate surface markers for rod cells will improve disease modeling using patient-specific iPS cells.

In brief, we generated pluripotent stem cells from retinitis pigmentosa patients and induced them into retinal cells. Compared with normal cells, patient-derived rod cells simulated the disease phenotype and exhibited different responses to specific drugs. We found that patient-specific rod cells underwent degeneration *in vitro*, which maybe related to different cellular stresses. To our knowledge, this is the first report of disease modeling of retinal degeneration using patient-derived iPS cells.

Supporting Information

Figure S1 Pedigrees of K21 (A), P59 (B), K10 and K11 (C). Families of P59 (**B**) and K10 and K11 (**C**) show autosomal dominant mode of inheritance. (**C**) Mutation analysis was performed in four patients and two normal relatives in the RP9 family. The H137L mutation in RP9 gene was co-segregated with the disease in the family. Closed symbols indicate individuals with RP and open symbols indicate unaffected subjects. Question marks indicate symptom unknown. The bars above the symbols indicate examined subjects. Arrow, proband; slash, deceased.
(TIF)

Figure S2 Mutation in the *RP9* gene. (**A**) Alignment of RP9 sequence and pseudo-gene shows the same nucleotide in the mutated location. (**B**) Sequence chromatogram of cDNA sequence demonstrates the c.410A>T (H137L) mutation in the *RP9* gene, instead of the paralogous variant in pseudo-gene which was documented in RetNet (www.sph.uth.tmc.edu/retnet/disease.htm).
(JPG)

Figure S3 Selection by colony morphology. (**A**) iPS colony (K21S4) shows ES-like morphology. (**B**) Spontaneous differentiation in the colony during maintenance (K21S14) Scale bars, 50 μm.
(TIF)

Figure S4 Quantification of transgene copy number. Total copy number of four transgenes in the selected iPS lines. Selected iPS cells with fewest integrations and two high copy number lines used for *in vitro* differentiation.
(TIF)

Figure S5 Efficiency of RPE induction in patient-iPS cells. RPE production of the five patient-iPS cells showed no significant differences (n = 4). Data represent the percentage of RPE area at differentiation day 60. One-way ANOVA followed by Dunnett's test. Values are mean and s.e.m.
(TIF)

Figure S6 Induced retinal cells from patient iPS cells (K21S4). Crx+ photoreceptor precursor cells present in the cell cluster on differentiation day 60 (A). Crx+ cells co-expressed Recoverin, indicating differentiation into photoreceptor cells (B). Rhodopsin+ cells had a long process at day 150 (C). In the differentiated cells, we also observed cells positive of PKCα (a marker for bipolar cells) (D). Cells positive for Math5 and Brn3b (markers for ganglion progenitor or ganglion cells (day 60) (E). Cells positive for Islet-1 (a marker for amacrine, bipolar and ganglion cells) (F). Scale bars, 50 μm (A, D, E, and F); 20 μm (B and C).
(TIF)

Figure S7 Differentiation of the patient-iPS cells. iPS colony was cut into uniform sized pieces (**A**) and subjected to a floating culture (P59M8, day 20) (**B**). RPE (pigmented) and recoverin+ (green) cells were efficiently induced (P59M8, day 60) (**C**). (**D**) An excluded iPS line, P59M16, with high number transgenes showed a striking lentoid formation during the floating culture (day 20). Scale bars, 50 μm.
(TIF)

Figure S8 Oxidative stress in photoreceptor cells with the RP9 mutation (K11). (A) Recoverin, (B) 8-OHdG, (C) Recoverin/8-OHdG, (D) Recoverin/8-OHdG/DNA. Arrows indicate cells with weak Recoverin signal positive for 8-OHdG; Arrowheads represent cells with strong Recoverin signal positive for 8-OHdG; Asterisks represent Recoverin+ cells negative for 8-OHdG. Scale bar, 50 μm.
(JPG)

Figure S9 ER stress in photoreceptor cells with the RHO mutation (P59). (A) CHOP, (B) Recoverin, (C) Recoverin/CHOP, (D) Recoverin/CHOP/DNA. Arrows indicate cells with weak Recoverin signals positive for CHOP in nuclei; Arrowheads represent cells with strong Recoverin signals positive for CHOP; Asterisks represent Recoverin+ cells negative for CHOP. Scale bar, 50 μm.
(JPG)

Figure S10 Toxicity testing of the antioxidants in murine retina-derived rod photoreceptor cells. Primary culture of mouse retinal cells treated with 100 μM α-tocopherol, 200 μM ascorbic acid or 1.6 μM β-carotene for 24 hours and the rod photoreceptors were counted using flow cytometry. Value represents the ratio of treated-rod photoreceptors compared with control cells. n = 4. One-way ANOVA followed by Dunnett's test. Values are mean and s.e.m. NS, not significant.
(JPG)

Figure S11 Differentiated rod cells from normal and patient iPS cells treated with 200 μM ascorbic acid or 1.6 μM β-carotene did not show statistically significant differences. Two-way ANOVA Bonferroni post-test. Values are mean and s.e.m.
(JPG)

Table S1 Phenotypic data of the RP patients. M, male; F, female; AD, age at diagnosis; BCVA, best corrected visual acuity; HM, hand motion.
(DOC)

Table S2 Antibodies used in the present study.
(DOC)

Acknowledgments

We thank C. Ishigami and Y. Tada for assistance of mutation screening; K. Iseki, N. Sakai, Y Wataoka, K. Sadamoto, A. Tachibana, C. Yamada for technical assistance; Y. Arata, W. Meng, C. Li, A. Suga, M. Mandai and all members in the Takahashi lab for advice.

Author Contributions

Conceived and designed the experiments: ZBJ MT. Performed the experiments: ZBJ SO FO KH JA. Analyzed the data: ZBJ SO FO. Contributed reagents/materials/analysis tools: MT YH TI. Wrote the paper: ZBJ MT.

References

1. Weleber RG, Gregory-Evans K (2006) Retinitis Pigmentosa and Allied Disorders. In: Hilton DR, Schachat AP, Ryan SJ, eds. Retina. Elsevier Mosby pp 395–498.
2. Berson EL, Rosner B, Sandberg MA, Hayes KC, Nicholson BW, et al. (1993) A randomized trial of vitamin A and vitamin E supplementation for retinitis pigmentosa. Arch Ophthalmol 11: 761–772.
3. Takahashi K, Tanabe K, Ohnuki M, Narita M, Ichisaka T, et al. (2007) Induction of pluripotent stem cells from adult human fibroblasts by defined factors. Cell 131 861–872.
4. Yu J, Vodyanik MA, Smuga-Otto K, Antosiewicz-Bourget J, Frane JL, et al. (2007) Induced pluripotent stem cell lines derived from human somatic cells. Science 318: 1917–1920.
5. Park IH, Arora N, Huo H, Maherali N, Ahfeldt T, et al. (2008) Disease-specific induced pluripotent stem cells. Cell 134: 877–886.
6. Raya A, Rodríguez-Pizà I, Guenechea G, Vassena R, Navarro S, et al. (2009) Disease-corrected haematopoietic progenitors from Fanconi anaemia induced pluripotent stem cells. Nature 460: 53–59.
7 Yamanaka S (2007) Strategies and new developments in the generation of patient-specific pluripotent stem cells. Cell Stem Cell 1: 39–49.
8. Osakada F, Ikeda H, Mandai M, Wataya T, Watanabe K, et al. (2008) Toward the generation of rod and cone photoreceptors from mouse, monkey and human embryonic stem cells. Nat Biotechnol 26: 215–224.
9. Osakada F, Jin ZB, Hirami Y, Ikeda H, Danjyo T, et al. (2009) In vitro differentiation of retinal cells from human pluripotent stem cells by small-molecule induction. J Cell Sci 122: 3169–3179.
10. Hirami Y, Osakada F, Takahashi K, Okita K, Yamanaka S, et al. (2009) Generation of retinal cells from mouse and human induced pluripotent stem cells. Neurosci Lett 458: 126–131.
11 Jin ZB, Mandai M, Yokota T, Higuchi K, Ohmori K, et al. (2008) Identifying pathogenic genetic background of simplex or multiplex retinitis pigmentosa patients: a large scale mutation screening study. J Med Genet 45: 465–472.
12. Ikeda H, Osakada F, Watanabe K, Mizuseki K, Haraguchi T, et al. (2005) Generation of Rx+/Pax6+ neural retinal precursors from embryonic stem cells. Proc Natl Acad Sci U S A 102: 11331–11336.
13. Sung CH, Davenport CM, Nathans J (1993) Rhodopsin mutations responsible for autosomal dominant retinitis pigmentosa. Clustering of functional classes along the polypeptide chain. J Biol Chem 268: 26645–26649.
14. van Leeuwen R, Boekhoorn S, Vingerling JR, Witteman JC, Klaver CC, et al. (2005) Dietary intake of antioxidants and risk of age-related macular degeneration. JAMA 294: 3101–3107.
15. van Helden YG, Keijer J, Heil SG, Picó C, Palou A, et al. (2009) Beta-carotene affects oxidative stress-related DNA damage in lung epithelial cells and in ferret lung. Carcinogenesis 30: 2070–2076.

Letter to the Editor

Stargardt Disease with Preserved Central Vision: identification of a putative novel mutation in ATP-binding cassette transporter gene

Kaoru Fujinami,[1] Masakazu Akahori,[2] Masaki Fukui,[1] Kazushige Tsunoda,[1] Takeshi Iwata,[2] and Yozo Miyake[1,3]

[1]Laboratory of Visual Physiology, National Institute of Sensory Organs, Meguro-ku, Tokyo, Japan
[2]Division of Molecular & Cellular Biology, National Institute of Sensory Organs, National Hospital Organization, Tokyo Medical Center, Meguro-ku, Tokyo, Japan
[3]Aichi Shukutoku University, Aichi, Japan, Nagakute-cho, Aichi-gun, Aichi, Japan

doi: 10.1111/j.1755-3768.2009.01848.x

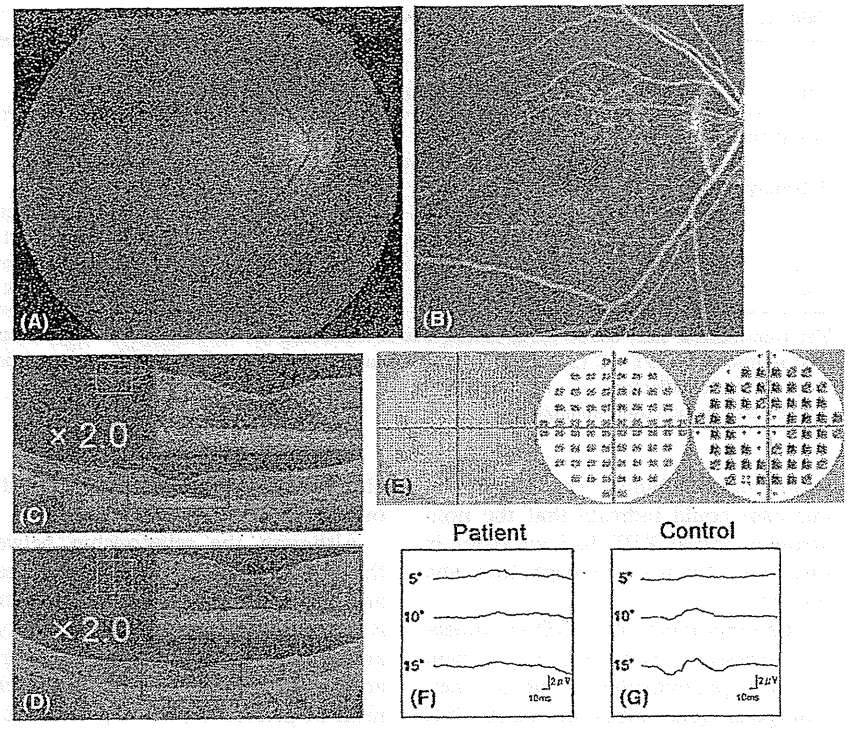

Fig. 1. Fundus photograph (A), fluorescein angiogram (FA) (B), optical coherence tomography (OCT) (C, D), Humphrey static perimetry (E), and focal macular electroretinograms (FMERGs) (F) of an eye of a patient with Stargardt disease. (A) Fundus photograph showing dark brown, well demarcated area in the fovea surrounded by orange-yellow flecks in the macula. (B) FA showing blockage in the foveal area, ring-shaped mottled hyperfluorescence in the macula, and dark choroid. (C, D) OCT images (C; horizontal, D; vertical) showing well-preserved sensory retina and retinal pigment epithelium (RPE) layer in the fovea. In the juxtafoveal region, an atrophy of both sensory retina and RPE can be seen. The enlarged images within the red lines are attached. (E) Humphrey static perimetry showing ring-shaped paracentral relative scotoma (10-2 strategy). (F, G) FMERGs showing normal responses elicited by a 5-degree stimulus spot and severely reduced responses elicited by 10-degree and 15-degree spots, when compared with the age-matched control.

Editor,

Stargardt disease (STGD) has a juvenile to young–adult onset, a rapid decrease of central vision and a progressive bilateral atrophy of the sensory retina and retinal pigment epithelium (RPE) in the macula. Yellow-orange flecks are often detected around the macula, the midretina and or both (Rotenstreich et al. 2003). Mutations in the gene encoding the ATP-binding cassette transporter gene (ABCA4) are responsible for autosomal recessive STGD (Allikmets 1997; Webster et al. 2001). We examined a patient who had the characteristic signs of STGD but had good visual acuity.

A 66-year-old man complained of photophobia and a paracentral scotoma which was present since his teens and had not worsened. None of his family members had similar symptoms. His visual acuity was 20/15 OU, and ophthalmoscopy identified a dark brown, well-demarcated area at the fovea surrounded by RPE atrophy and flecks (Fig. 1A). Fluorescein angiography showed window defects at the flecks and a dark choroid (Fig. 1B). The optical coherence tomographic (OCT) images showed a well-preserved sensory retina and normal thickness RPE at the fovea (Fig. 1C, D). The foveal area was surrounded by atrophic sensory retina and RPE. Static perimetry showed ring-shaped paracentral relative scotoma which surrounded the normal area seeing area of 5° (Fig. 1E). Focal macular electroretinograms (FMERGs) also demonstrated a well-preserved retinal function at the fovea (Fig. 1F). Compared to age-matched controls, the FMERGs had normal responses elicited by a 5-degree stimulus spot and severely reduced responses elicited by 10-degree and 15-degree spots (Fig. 1F, G). Genetic analysis with direct DNA sequencing of amplified products revealed four reported polymorphisms (Allikmets 1997; Briggs et al. 2001; Webster et al. 2001; Fukui et al. 2002) and one novel mutation, Met280Thr, in exon 7 of the ABCA4 gene (Table 1).

Our patient had clinical findings that were pathognomonic of typical STGD, except that the clinical course was stationary and he had 20/15 vision because of well-preserved foveal function. The preserved foveal area was small and well demarcated. Visual acuity, fundus appearance, OCT images, static perimetry and FMERGs supported the well-preserved foveal function. We report our case because the patient had a unique phenotype with a novel putative mutation in the *ABCA4* gene, not yet shown to segregate with the disease.

The well-demarcated dark brown foveal RPE appeared to be hyperpigmented although the thickness measured by OCT was 29 μm which was

Table 1. ABCA4 GENE MUTATION AND Polymorphisms.

Exon	Nucleotide Change	Effect Changes	Het/Hom	References
Mutation				
7	c.839T>C	p.Met280Thr	Het	Present study
Polymorphisms				
10	c.1269C>T	p.His424His	Hom	Webster AR et al.
45	c.6249C>T	p.Ile2083Ile	Het	Allikmets R et al.
46	c.6285T>C	p.Asp2095Asp	Het	Briggs CE et al.
49	c.6764G>T	p.Ser2255Ile	Het	Allikmets R et al.

The translational start codon ATG/methionine is numbered as +1. One novel disease-associated mutation [c.839T>C (p.Met280Thr)] was found. References of previously reported polymorphisms are indicated.
Het, heterozygote; Hom, homozygote.

within normal limits. The findings in our case could indicate that the non-atrophic foveal RPE had an effect in preserving the foveal morphology and function.

The inheritance of STGD is autosomal recessive; however, our patient had four polymorphisms and one heterozygous gene mutation c.839T>C in exon 7 in the *ABCA4* gene. A second mutation was not found, but it may well exist outside of the coding sequence of the *ABCA4* gene. The new mutation in our patient was located outside the known functional domains of ATP-binding or transmembrane site (Lewis et al. 1999), which may explain the mild effect of the missense mutation. We should also consider a modifier gene effect in our patient.

Although the relationship between the new mutation of the *ABCA4* gene and the well-preserved foveal structure is unresolved, the unique phenotype and genotype of our patient may give additional information on the mechanism of photoreceptor degeneration in eyes with STGD.

References

Allikmets R (1997): A photoreceptor cell-specific ATP-binding transporter gene (ABCR) is mutated in recessive Stargardt macular dystrophy. Nat Genet **17**: 122.

Briggs CE, Rucinski D, Rosenfeld PJ, Hirose T, Berson EL & Dryja TP (2001): Mutations in ABCR (ABCA4) in patients with Stargardt macular degeneration or cone-rod degeneration. Invest Ophthalmol Vis Sci **42**: 2229–2236.

Fukui T, Yamamoto S, Nakano K et al. (2002): ABCA4 gene mutations in Japanese patients with Stargardt disease and retinitis pigmentosa. Invest Ophthalmol Vis Sci **43**: 2819–2824.

Lewis RA, Shroyer NF, Singh N et al. (1999): Genotype/Phenotype analysis of a photoreceptor-specific ATP-binding cassette transporter gene, ABCR, in Stargardt disease. Am J Hum Genet **64**: 422–434.

Rotenstreich Y, Fishman GA & Anderson RJ (2003): Visual acuity loss and clinical observations in a large series of patients with Stargardt disease. Ophthalmology **110**: 1151–1158.

Webster AR, Heon E, Lotery AJ et al. (2001): An analysis of allelic variation in the ABCA4 gene. Invest Ophthalmol Vis Sci **42**: 1179–1189.

Correspondence
Kazushige Tsunoda, MD
Laboratory of Visual Physiology
National Institute of Sensory Organs
2-5-1 Higashigaoka
Meguro-ku
Tokyo 152-8902
Japan
Tel: + 81 3 3411 0111 ext. 6615
Fax: + 81 3 3412 9811
Email: tsunodakazushige@kankakuki.go.jp

Exp. Anim. 59(2), 171–182, 2010

—Original—

Comparative Proteomic Analyses of Macular and Peripheral Retina of Cynomolgus Monkeys (*Macaca fascicularis*)

Haru OKAMOTO[1, 2], Shinsuke UMEDA[1], Takehiro NOZAWA[3], Michihiro T. SUZUKI[4], Yasuhiro YOSHIKAWA[5], Etsuko T. MATSUURA[6], and Takeshi IWATA[1]

[1]Division of Molecular & Cellular Biology, National Institute of Sensory Organs, National Hospital Organization Tokyo Medical Center, 2–5–1 Higashigaoka, Meguro-ku, Tokyo 152-8902, Japan, [2]Department of Advanced Biosciences, Ochanomizu University, 2–1–1 Otsuka, Bunkyo-ku, Tokyo 112-8610, Japan, [3]Analytical Instrument Division, AMR Inc., 2–13–18 Nakane, Meguro-ku, Tokyo 152-0031, Japan, [4]The Corporation for Production and Research of Laboratory Primates, 1–1 Hachimandai, Tsukuba-shi, Ibaraki 305-0843, Japan, [5]Department of Biomedical Science, Graduate School of Agricultural and Life Sciences, The University of Tokyo, 1–1–1 Yayoi, Bunkyo-ku, Tokyo 113-8657, Japan, and [6]The Natural/Applied Sciences Division, Ochanomizu University, 2–1–1 Otsuka, Bunkyo-ku, Tokyo 112-8610, Japan

Abstract: The central region of the primate retina is called the macula. The fovea is located at the center of the macula, where the photoreceptors are concentrated to create a neural network adapted for high visual acuity. Damage to the fovea, e.g., by macular dystrophies and age-related macular degeneration, can reduce central visual acuity The molecular mechanisms leading to these diseases are most likely dependent on the proteins in the macula which differ from those in the peripheral retina in expression level. To investigate whether the distribution of proteins in the macula is different from the peripheral retina, proteomic analyses of tissues from these two regions of cynomolgus monkeys were compared. Two-dimensional gel electrophoresis and mass spectrometry identified 26 proteins that were present only in the macular gel spots. The expression levels of five proteins, cone photoreceptor specific arrestin-C, γ-synuclein, epidermal fatty acid binding protein, tropomyosin 1α chain, and heterogeneous nuclear ribonucleoproteins A2/B1, were significantly higher in the macula than in the peripheral retina. Immunostaining of macula sections by antibodies to each identified protein revealed unique localization in the retina, retinal pigment epithelial cells and the choroidal layer. Some of these proteins were located in cells with higher densities in the macula. We suggest that it will be important to study these proteins to determine their contribution to the pathogenesis and progression of macula diseases.

Key words: 2D-gel electrophoresis, macula, mass spectrometry, retina

(Received 16 September 2009 / Accepted 13 November 2009)

Address corresponding: T. Iwata, Division of Molecular & Cellular Biology, National Institute of Sensory Organs, National Hospital Organization Tokyo Medical Center, 2–5–1 Higashigaoka, Meguro-ku, Tokyo 152-8902, Japan

Introduction

The macula is an oval-shaped, highly pigmented spot near the central region of the primate retina. It is approximately 2.0 mm in diameter in humans [31] and 1.0 mm in macaque monkeys [36–38]. The fovea is located at the center of macula where the retinal thickness is reduced to approximately 0.1 mm and consists of only the retinal pigment epithelium (RPE), photoreceptor layer, external limiting membrane, outer nuclear layer, outer plexiform layer, and inner limiting membrane [30]. The cone density in the foveal pit is the highest in the retina, and rods, retinal ganglion cells (RGCs), and blood vessels are not present. These cones are connected to large numbers of RGCs, which are highly dense at the parafovea [31]. The cone-dense fovea mediates high-acuity central vision, and any damage to the macula can lead to severely depressed central visual acuity as observed in patients with macular dystrophies and age-related macular degeneration (AMD).

Because of the unique cellular organization of the macula, investigators have performed comprehensive gene expression studies of the macula and peripheral retina using DNA microarray analysis or Serial Analysis of Gene Expression (SAGE). Sharon *et al.* used SAGE to show that several genes are preferentially expressed in the human macula and RPE. Most of these genes are associated with the function of the RGCs, and were presumably detected because of the high density of RGCs in the macula [35]. Bowes Rickman *et al.* also performed SAGE on human retinas and isolated RPE cells and identified genes that are abundantly expressed in cones, RGCs, and RPE cells [3]. Ishibashi *et al.* performed 4 K DNA microarray analysis on RPE cells from the macula and reported five differentially expressed genes which were confirmed by real-time PCR [18]. Recently, Radeke *et al.* [32] and van Soest *et al.* [48] used 22 K DNA microarray analyses and identified a number of genes that were differentially expressed in the macula and peripheral retina. In each study, five of these genes were found to be highly expressed in RPE cells in the macula. van Soest *et al.* showed by immunohistochemistry that the WAP four-disulfide core domain 1, one of the highly expressed proteins, is present in the RPE cells in the macula. However, the expression level of the mRNAs does not always correlate with the expression levels of the proteins.

Recent technical advances in proteomics allow the direct determination of the protein profile of body fluids and tissue homogenates. Proteomic analyses of the retina were first performed by Nishizawa *et al.* [28], and several groups have catalogued the retinal proteins using single or two-dimensional (2D) gel electrophoresis followed by mass spectrometry (MS) analysis [1, 5, 50]. Ethen *et al.* examined cadaver eyes with AMD by proteomic analyses and reported that the expression of proteins changed with the progression of AMD, and the changes in the macula were different from those in the peripheral retina [10]. These findings indicate that the macular region of the retina is different from the peripheral retina not only in its morphology but also in its protein content.

Proteomic studies of the macula are difficult to perform because of the lack of fresh human eyes, and small sample size of the macula. To overcome these problems, we selected non-human primate eyes of the cynomolgus monkey (*Macaca fascicularis*). The retina and visual system of macaque monkeys are quite similar to those of humans [14, 29], and monkeys with characteristics of macular diseases have been reported by many investigators [9, 16, 19, 25, 39, 40] as well as our previous studies [26, 27, 44–47]. Thus, the purpose of this study was to identify proteins present at high levels in the macula to better understand the biology of this unique tissue. To accomplish this task, we performed proteomic analyses on retinal tissues obtained from the macular region and the periphery for comparison.

Materials and Methods

Preparation of cynomolgus monkey eyes

All experiments on monkeys were approved by the Animal Ethics Committee of the Tsukuba Primate Research Center (TPRC) and were conducted in accordance with The Association for Research in Vision and Ophthalmology Statement for the Use of Animals in Ophthalmic and Vision Research. Eight eyes from eight normal female cynomolgus monkeys (*Macaca fascicularis*) whose ages ranged between 13 to 19 years were studied. Eyes were removed approximately one hour

after death and treated with RNAlater (Applied Biosystems, Tokyo, Japan). Other tissues from these animals were used by other research groups at the TPRC. Three-millimeter-diameter pieces of macular and peripheral retina containing neural retina, RPE and choroidal layer were punched out and frozen until use. The proteins extracted from the tissues of eight eyes were pooled for the analyses.

Protein extraction and 2D-gel electrophoresis

The proteins from the macula and peripheral retina were extracted after homogenization and sonication in sample buffer [7 M urea, 2 M thiourea, 4% CHAPS, 50 mM DTT, 40 mM Tris, 0.2% Bio-Lyte 3/10 (Bio-Rad, Hercules, CA, USA)]. After centrifugation for 15 min × 3 at 14,000 rpm (20,800 × *g*), the supernatant was collected. The lysate was precipitated using Ready Prep 2D cleanup kit (Bio-Rad) and redissolved in sample buffer. The protein concentration was determined with the RC-DC protein assay kit (Bio-Rad) according to the manufacturer's instruction. Protein samples (300 μg) were separated by isoelectric focusing (IEF) using 17-cm immobilized pH gradient (IPG) strips. After 12 to 16 h of rehydration at 20°C, the IEF sample was used for the first dimension with an initial voltage of 250 V for 15 min and then increased to 10,000 V for 3 h and held until 60,000 V-h was reached. Immediately after the IEF, the IPG strips were stored at –20°C until the equilibration step was carried out. The IPG strips were equilibrated for 20 min in buffer containing 6 M urea, 2% SDS, 0.375 M Tris (pH 8.8), and 20% glycerol under reduced conditions with 2% DTT, followed by another incubation for 10 min in the same buffer under alkylating conditions with 2.5% iodoacetamide. The equilibrated IPG strips were electrophoresed for the second dimension using 12% acrylamide gels. Two dimensional gel electrophoresis was performed at four different pH ranges, viz., pH 3–10, 4–7, 5–8, and 7–10. After the 2D gel electrophoresis, the proteins were stained with SYPRO Ruby (Bio-Rad). The images for the macula and peripheral retina were compared with ImageMaster 2D Platinum ver.5.0 (GE Healthcare Bio-Sciences, Piscataway, NJ, USA) followed by visual inspection. The gel spots numbered in Fig. 1 were excised. Two dimensional gels of peripheral retina were stained with Bio-safe Coomassie (Bio-Rad). Then, 46 spots from the Coomassie-stained gel were excised (Fig. 1, Peripheral Coomassie).

In gel digestion and LC-MS/MS analyses

Each gel piece was cut into approximately one cubic millimeter and washed twice with 50 mM ammonium bicarbonate/50% acetonitrile. After destaining, the gel pieces were rinsed with distilled water, and incubated with acetonitrile for 20 min. The supernatant was discarded and the gel pieces were completely dried before incubation with 10 mM DTT in 100 mM ammonium bicarbonate for 45 min at 56°C. The supernatant was discarded and the pieces were incubated in the dark with 55 mM iodoacetamide in 100 mM ammonium bicarbonate (30 min, at room temperature). The supernatant was discarded, and the gels were washed three times. Finally, the gel pieces were completely dried before tryptic digestion in sequencing grade trypsin solution (12.5 ng/μl; Promega, Madison, WI, USA) in 50 mM ammonium bicarbonate. The digestion was performed at 37°C overnight, and the extraction step was performed once with 25 mM ammonium bicarbonate, twice with 5% formic acid, and finally with distilled water. The extracted peptides were pooled and dried. After re-suspending in 40 μl of aqueous 0.01% trifluoroacetic acid/2% acetonitrile, the samples were analyzed by LC (liquid chromatography)-MS/MS. LC-MS/MS was performed with a combined Paradigm MS4 (Michrom BioResources, Auburn, CA, USA) and an ESI mass spectrometer (LCQ Deca XP plus or Finnigan LTQ, Thermo Fisher Scientific, Yokohama, Japan; assembled by AMR Inc., Tokyo, Japan). For the LCQ analysis, sample peptides were separated in nano column (AMR Inc.) with solvent A (2% acetonitrile/0.1% formic acid) and B (90% acetonitrile/0.1% formic acid) at flow rate of 0.6 μl/min, gradient of 5 to 95% solvent B over 40 min. For the LTQ analysis, peptides were separated on Magic C18 (Michrom BioResources) with solvent A and B, a flow rate 1.5 μl/min, gradient of 5 to 95% solvent B over 30 min. The identification of the proteins from the MS/MS spectra was performed using protein identification software (Bioworks ver.3.1, Thermo Fisher Scientific) and UniProtKB/Swiss-Prot database (Release 48.8) which was preliminarily extracted by the species "human" (13,361 entries). Peak list generation and database searches were performed with the following

parameters: mass tolerance for precursor ions, 2.5 amu; mass tolerance for fragment ions, 0.00 amu; enzymatic cleavage position, after lysine or arginine; number of missed cleavage sites permitted, 2; fixed modification, carbamide-methylation (+57.02 Da) for cysteine; variable modification, oxidation (+16 Da) for methionine. The peptide sequences were filtered by delta Cn score and peptide Cross Correlation (XC) score. The threshold level of delta Cn scores was >0.1 for peptide sequences from both measurement devices. The threshold levels of XC scores for each charge (+1/+2/+3) were >1.5/2.0/3.7 for LCQ and >1.9/2.2/3.7 for LTQ. Then, the correlations between the observed in gel images and the theoretical molecular weight and pI were considered. When peptides matched multiple members of the protein family, the protein which had the most number of peptides that matched the amino acid sequence was selected. In case of equal numbers, both proteins were listed.

Western blotting and immunohistochemical analysis of macula

Five to fifteen micrograms of macula or peripheral retinal homogenates were diluted in a double volume of SDS buffer and separated by 1D-PAGE followed by transfer to PVDF (polyvinylidene difluoride) membrane. Membranes were blocked with blocking solution (Blocking Solution Concentrate, KPL, Gaithersburg, MD, USA), skim milk, or BSA dissolved in PBS and probed with one of the following primary antibodies (Abs): chicken Ab to human arrestin-C (GenWay Biotech, San Diego, CA, USA), rabbit Ab to human synuclein gamma (Novus Biologicals, Littleton, CO, USA), rat Ab to human epidermal fatty acid binding protein (E-FABP) (R&D Systems, Minneapolis, MN, USA), rabbit Ab to tropomyosin Br-1, Br-3 (CHEMICON International, Temecula, CA, USA), mouse Ab to chicken tropomyosin TM311 (Abcam, Cambridge, UK), and goat Ab to human heterogeneous nuclear ribonucleoproteins (hnRNPs) A2/B1 (Santa Cruz Biotechnology, Santa Cruz, CA, USA). The specific signals were detected with one of the following secondary antibodies: horseradish peroxidase (HRP)-conjugated goat Ab to mouse IgG (Jackson ImmunoResearch Laboratories, West Grove, PA, USA), HRP-conjugated goat Ab to rabbit IgG (Pierce, Rockford, IL, USA), HRP-conjugated rabbit Ab to chicken/turkey IgG (Zymed Laboratories, South San Francisco, CA, USA), HRP-conjugated donkey Ab to goat IgG (Jackson ImmunoResearch Laboratories), HRP-conjugated goat Ab to rat IgG (Zymed Laboratories). The signals were made visible by chemiluminescence reactions and examined with a chemiluminescence imager (Lumi-Imager F1; Roche Diagnostics, Tokyo, Japan). An enucleated eye from a normal female cynomolgus monkey (age 13 years) was fixed in 10% neutralized and buffered formaldehyde solution at 4°C overnight and then dehydrated. The specimens were embedded in paraffin and serially sectioned at 4 μm thickness. The specimens were treated for antigen retrieval by autoclaving in Target Retrieval Solution (Dako, Carpinteria, CA, USA) for 20 min at 121°C. The sections were then blocked with Dako Protein Block (Dako) or skim milk or BSA in PBS. The primary antibodies were the same as used for the western blotting, and rabbit Ab to human platelet/endothelial cell adhesion molecule (PECAM1) (Proteintech Grroup, Chicago, IL, USA). For signal detection after rinsing off the primary antibodies, the sections were incubated with one of following secondary antibodies: Alexa 488-conjugated goat Ab to anti-mouse IgG, Alexa 568-conjugated goat Ab to anti-mouse IgG, Alexa 488-conjugated goat Ab to anti-rabbit IgG, Alexa 568-conjugated goat Ab to anti-rabbit IgG, Alexa 488-conjugated donkey Ab to anti-goat IgG, Alexa 568-conjugated goat Ab to anti-chicken IgG, and Alexa 488-conjugated goat Ab to anti-rat IgG (all secondary antibodies from Invitrogen, Tokyo, Japan). After rinsing off the antibodies, the sections were examined by confocal laser scanning microscope (Radiance 2100, Bio-Rad). The cell nuclei were stained with DAPI (4',6-diamino-2-phenylindole). To determine the location of the signals, one of the sections was stained with hematoxylin and eosin.

Results

Identification of macula enriched proteins

Approximately 700 spots were detected in the macular and peripheral retinal tissues in the 2D gel stained with SYPRO Ruby (pH range 3–10; Fig. 1A). Sixty percent of these spots were found in both samples. Butt *et al.* have described the difficulties of IEF separation by RNAlater contaminations [4]. Our samples were de-

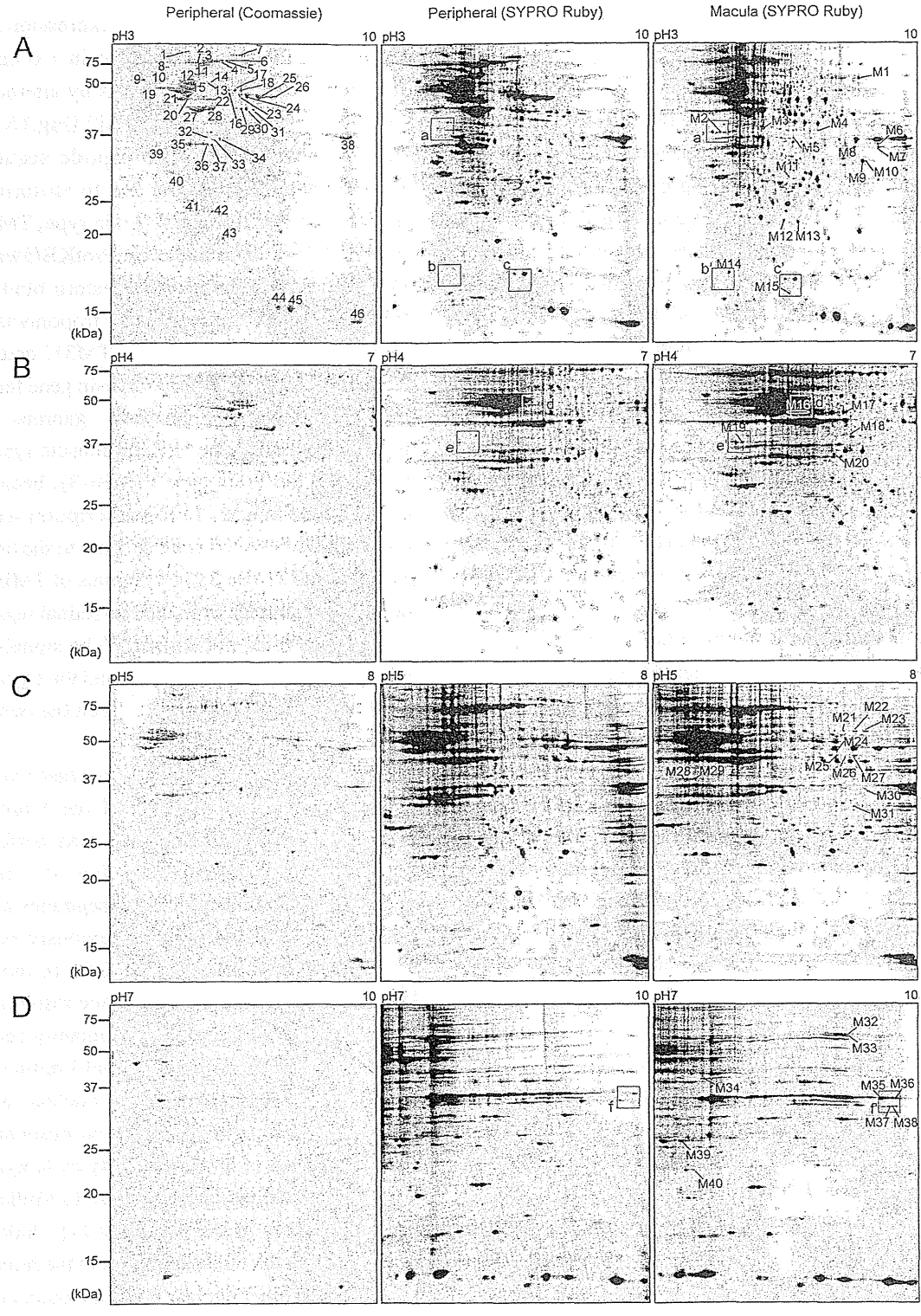

Fig. 1. Separation of monkey retina proteins on 2D gels Proteins extracted from the peripheral retina and macula (300 μg each) were isoelectric focused at four different pH ranges; pH 3–10 (A), 4–7 (B), 5–8 (C), 7–10 (D) Then the IPG strips were separated on 12% SDS-page gels and stained by SYPRO Ruby. Forty spots marked by spot IDs were unique to the macula gel images and identified by LC-MS/MS Boxed areas (a–f, Peripheral-SYPRO Ruby; a'–f', Macula-SYPRO Ruby) correspond to the enlarged images in Fig 2 Two dimensional gels of peripheral retina were also stained by Bio-safe Coomassie Forty-six spots marked by spot number were identified by LC-MS/MS.

salted prior to the IEF separation by Ready Prep 2D cleanup kit using TCA (trichloroacetic acid) acetone precipitation which resulted in successful separations. To obtain a further separation, the pH range of the 2D gel electrophoresis was narrowed to three ranges; 4–7, 5–8, and 7–10 (Fig. 1B–D). Among gel images for both the macula and peripheral retina, fluorescence from spots of abundant proteins were saturated and showed indistinct spot boundaries. Excess proteins contained in the samples were not concentrated at one spot by 2D gel electrophoresis and showed streaking and outliers. To exclude these proteins which were identified from seemingly macular specific spots, abundant proteins were identified. To clarify the outline of saturated spots, gels of peripheral retina were stained with Bio-safe Coomassie. Forty-nine proteins were identified from forty-six spots in the Coomassie stained gel image of the pH 3–10 range (Fig. 1A, Peripheral Coomassie). The proteins are listed in Table 1. Forty-eight known proteins from earlier proteomic studies of the retina were identified [1, 5, 15, 49, 50]. The neurofilament triplet L protein identified in our study has not been previously identified by the proteomic approach but it has been reported in a SAGE analysis [35]. The 49 proteins were expressed in both the macula and peripheral retina, while 26 proteins were identified from 40 spots in macula gel images (Table 2). Twenty-three of these were also reported in previous proteomic studies of the retina [1, 5, 10, 15, 22, 50]. The other three proteins are known to be ubiquitously expressed in cells [8, 11]. Therefore, these proteins were not macula specific but widely expressed in the retina.

Validation of macula enriched proteins

To obtain the relative expression levels of the identified proteins, western blot analysis was performed on the following five proteins identified by mass spectrometry: tropomyosin 1 α chain (Fig. 2A and 2E), γ-synuclein (Fig. 2B), E-FABP (Fig. 2C), arrestin-C (Fig. 2D), and hnRNPs A2/B1 (Fig. 2F). Arrestin-C has been identified as a cone photoreceptor-specific protein [33], and thus served as a positive control for this study. γ-Synuclein is a protein known to be up-regulated in cancer cells [20]. hnRNPs A2/B1 is also known to be up-regulated in carcinoma cells [42]. E-FABP is a reactive lipid scavenger [2]. Four proteins, including arrestin-C, were confirmed to have higher expression in the macula by western blotting. Tropomyosin 1 α chain has been reported to have many isoforms by alternative splicing [34]. MS/MS data from spot M2 (Fig.1A, Macula SYPRO Ruby) identified the peptide sequence CAELEEELK, which corresponded to isoform 1 (skeletal muscle type) or isoform 5 (brain type, TMBr-3) of tropomyosin 1 α chain in the UniProtKB/Swiss-Prot database. Based on these data, western blotting was performed using two antibodies for tropomyosin 1 α chain. The anti-tropomyosin antibody TM311 detects 19 amino acids in exon 1a of the tropomyosin gene family in mammalian tissues, viz., alpha-, beta-, gamma-, delta- tropomyosin, including the skeletal muscle type but it does not detect the brain type (TMBr-3), because TMBr-3 doesn't contain exon 1a in transcription sequence. The other antibodies used were specific to the brain isoforms TMBr-1 and TMBr-3 [34]. Signals of TMBr-1 were not detected in samples from the two retinal regions by western blotting (data not shown). The signals of TMBr-3 were not significantly different, and the signals to TM311 were found to be different between the two regions.

Tissue localization of macula enriched proteins

To determine the location of the 5 proteins in the macula, immunohistochemistry was performed using antibodies against each protein (Fig. 3). Arrestin-C was detected in photoreceptor outer segments and the outer plexiform layer (Fig. 3B) as previously reported [33]. γ-Synuclein was detected in RGCs in the nerve fiber layer (Fig. 3D), which confirms the result of a previous study [43]. E-FABP was predominantly detected in the outer plexiform layer and external limiting membrane, which exists between the outer nuclear layer and the photoreceptor layer (Fig. 3G). Our observation is consistent with that of an earlier study by Kingma *et al.* reporting the localization of E-FABP to Müller cells [21], which are dense in the parafovea [7]. hnRNPs A2/B1 was located in the nucleus of cells in the retinal ganglion cell layer, the inner nuclear layer, the outer nuclear layer, and the RPE with different intensities (Fig. 3E). TM311 was detected in the choroidal layer (Fig. 3F), while tropomyosin Br-3 was located in photoreceptor inner segments and the outer plexiform layer (Fig. 3C). To determine the localization of tropomyosin detected by TM311